The Budget of Turbulent Energy Measured at the ERC 30-m Meteorological Tower

By Kenji Kai

The Environmental Research Center, the University of Tsukuba, Ibaraki, 305 Japan
(Manuscript received 31 October 1981, in revised form 15 June 1982)

Abstract

Turbulence measurements of wind and temperature were made by sonic anemometer-thermometers in the first thirty meters of the atmosphere. Turbulent statistics obtained by direct measurements were analyzed, using the Monin-Obukhov similarity theory.

The behaviors of the terms in the turbulent energy budget were examined, together with the relation of turbulent statistics to the measured parameters such as mean wind speed, stability and height. A model of the turbulent energy budget was derived from the results. Under near neutral conditions, mechanical production and viscous dissipation are dominant and essentially in balance, while turbulent transport and buoyant production are not important. In unstable conditions, each term in the budget is important. Buoyant production is a gain and turbulent transport is a loss. In stable conditions, all terms except turbulent transport are significant. Mechanical production and the imbalance are the sources of turbulent energy and the others energy sinks. For both stable and unstable conditions, the imbalance increases with the magnitude of stability.

1. Introduction

The structure of atmospheric turbulence reflects the budget of production, transport and dissipation of turbulent energy. So, the budget of turbulent energy is of special importance. In the surface boundary layer, production of turbulent energy by both wind shear and buoyancy plays a primary role, and is concentrated in the region very near the ground.

The equation for the turbulent energy budget may be written for the case of horizontally homogeneous turbulence (see Lumley and Panofsky, 1964),

$$\underset{(TE)}{\frac{\partial}{\partial t}\frac{\overline{q^2}}{2}} = \underset{(MP)}{-\overline{uw}\frac{\partial \bar{U}}{\partial z}} + \underset{(BP)}{\frac{g}{\bar{T}}\overline{w\theta}} \underset{(TT)}{-\frac{\partial}{\partial z}\frac{\overline{wq^2}}{2}} - \underset{(PT)}{\frac{\partial}{\partial z}\frac{\overline{wp}}{\rho}} \underset{(VD)}{-\varepsilon} \qquad (1)$$

where u, v, w are the three components of the wind fluctuation ($\bar{u}=\bar{v}=\bar{w}=0$) in directions x, y, z, respectively; $\bar{U}$ is the mean wind speed; θ, p are the fluctuating temperature and pressure, respectively; $q^2=u^2+v^2+w^2$ is twice the turbulent energy per units mass; $\bar{T}$ and ρ are the means of temperature and density of the air; g is the acceleration due to gravity; and ε is the rate of viscous dissipation of turbulent energy. The terms in Eq. (1) can be identified as (from the left) the rate of change of turbulent energy *TE*, mechanical production *MP*, buoyant production *BP*, turbulent transport *TT*, pressure transport *PT*, and viscous dissipation *VD*. Fig. 1 shows a schematic diagram of the turbulent energy

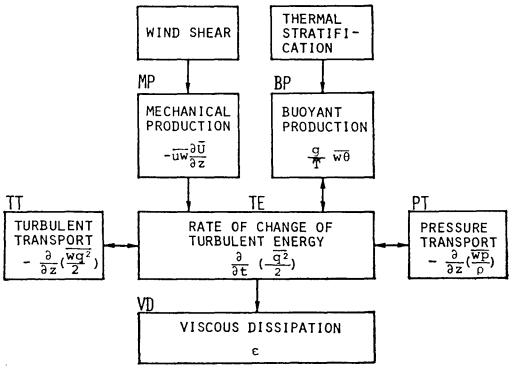

Fig. 1 Schematic diagram of the turbulent energy budget.

Table 1 Summary of various experiments associated with the turbulent energy budget.

Observer	Location	Type of terrain	Heiget of measurement (m)	Sensor	Averaging time (sec)	Duration (min)	Stability	Comments
Panofsky, 1962	Brookhaven, N.Y.	Scrub pine	23, 46, 91	Aerovane Bivane	5	60	All	
Lenschow, 1970	Colorado	Flat treeless area	100, 200, 450, 1,000	Incidence angle vane, Pitot-static tube	0.03	5	Unstable	Vertical structure
McBean et al., 1971	Vancouver	Mown grass	2	SAT Hot-wire	0.0125	15	Unstable Neutral	
Wyngaard & Coté, 1971	Kansas	Uniform wheat	5.66, 11.3, 22.6	SAT Hot-wire	0.05	60	Unstable	T.E.B. model
Garratt, 1972	Lough Neagh, Northern Ireland	Over water	1.4, 4, 12	Bivane Hot-wire	0.1	15	All	ε vs. z/L
Monji, 1973	Bonneville, Utah	Salt crystal	4.2, 15	SAT Thermocouple		40	Unstable	
Lenschow, 1974	Colorado, L. Michigan L. Huron	Over water Homogeneous surface	100–1,000	Incidence angle vane, Pitot-static tube	0.03	5	Unstable Neutral	Model of height variation of T.E.B.
McBean & Elliott, 1974	Suffield, Alberta	Prairie grass	5.77	SAT	0.05	250	Unstable	Spectral model Pressure transport
Rayment & Caughey, 1977	Earles Croome, England	Rural	61, 91, 152	Cardington turbulence probe		120	Unstable	Time change
Maitani, 1977	Kojima Bay	Paddy field	1.2, 3	SAT	0.17	30	Unstable	
Yamamoto, 1977	Kawaguchi	Urban	20, 45, 90, 180, 313	SAT	0.05–2.5	8.3–40	Stable	
Campagne, 1977	Minnesota	Flat farmland	4, 32	SAT Hot-wire	0.06	60(15)	Unstable Neutral	
Caughey & Wyngaard, 1979	Minnesota	Flat farmland	1, 2, 4, 8, 16, 32, 61–1,219	SAT MRU turbulence probe	0.1	75	Unstable	
The present study	Tsukuda	Grass about 50 cm tall	1.6, 4.3, 12.3, 29.5	SAT	0.05	30	All	T.E.B. model Vertical structure

budget.

The main purpose is to investigate the turbulent energy budget over a wide range of stability conditions in the surface boundary layer. In order to carry out the purpose, turbulence measurements of wind and temperature were made in the first thirty meters of the atmosphere. Four sonic anemometer-thermometers were used for turbulence measurements. In the present study it is possible to specify relative magnitudes of the terms in the turbulent energy budget.

Over the past two decades, there have been several experimental studies of the turbulent energy budget in the surface boundary layer, as summarized in Table 1. In spite of these studies, there is still not complete agreement on the relative importance of each term in the turbulent energy budget.

Panofsky (1962) suggested that the flux of turbulent energy was upward and that turbulent transport was an important term in the budget equation under unstable conditions. Busch and Panofsky (1968), however, concluded that viscous dissipation was balanced by mechanical and buoyant production and that turbulent transport was unimportant in the case of homogeneous terrain.

Instrumented aircrafts were used to estimate directly the budget of turbulent energy in the planetary boundary layer by Lenschow (1970, 1974). Lenschow (1970) reported that viscous dissipation was almost constant with height between the lowest flight level of 100 m above the ground, and the highest flight level of 1000 m, which was just below the top of the planetary boundary layer, while turbulent transport increased with height to balance the decrease in buoyant production. Lenschow (1974) proposed a model of the height variation of the turbulent energy budget in the unstable planetary boundary layer.

In 1968, the Boundary Layer Branch of the Air Force Cambridge Research Laboratories carried out an extensive and systematic study of the surface boundary layer at a site in Kansas (Haugen, 1973; Wyngaard and Coté, 1971). Based on the Kansas experiments, Wyngaard and Coté (1971) made a detailed study of the turbulent energy budget. They concluded that for unstable conditions, viscous dissipation is balanced by mechanical production and an imbalance, and that buoyant production and turbulent transport are approximately in balance. They suggested that the imbalance may be ascribed either to pressure transport (which was not measured) or to experimental difficulties such as horizontal inhomogeneity.

Recent studies of the turbulent energy budget confirmed the existence of the imbalance and relate this to pressure transport (McBean and Elliott, 1975; Champagne et al., 1977; Caughey and Wyngaard, 1979). Pressure transport has been measured directly by Elliott (1972). His results indicated that pressure transport was about one-tenth of mechanical production for near neutral conditions, but no measurements were made for stable and unstable conditions. McBean and Elliott (1975) examined the transport of turbulent energy by turbulence and pressure for a surface boundary layer over a dry prairie grassland. They found that for unstable conditions turbulent transport was about equal to minus buoyant production, and that pressure transport was of opposite sigh and of about equal magnitude to turbulent transport.

McBean et al. (1971) reported that for slightly unstable conditions the total production was balanced by viscous dissipation and that for more unstable conditions viscous dissipation exceeded the production. Garratt (1972) found that viscous dissipation and turbulent transport was significant on occasions but small on the average. From the standpoint of the budget relations of turbulent energy and temperature variance, Monji (1973) discussed the transition from the surface layer to the free convection layer of the unstable planetary boundary layer. Maitani (1977) showed the characteristics of the turbulent transport and viscous dissipation were the main loss terms under unstable conditions and that these terms increased in magnitude with instability.

Theoretical studies have shown qualitative characteristics of turbulence to a certain degree, but not for quantitative ones. Experimental studies are necessary for acquiring information with regard to the quantitative characteristics. The results by Wyngaard and Coté (1971) was unique in providing direct measurements of all terms except pressure transport in the turbulent energy budget. Wyngaard and Coté established the model of the turbulent energy budget for unstable conditions, but a general specification of the turbulent energy budget including the case of stable conditions has not yet been achieved. The emphases in this study will be on the be-

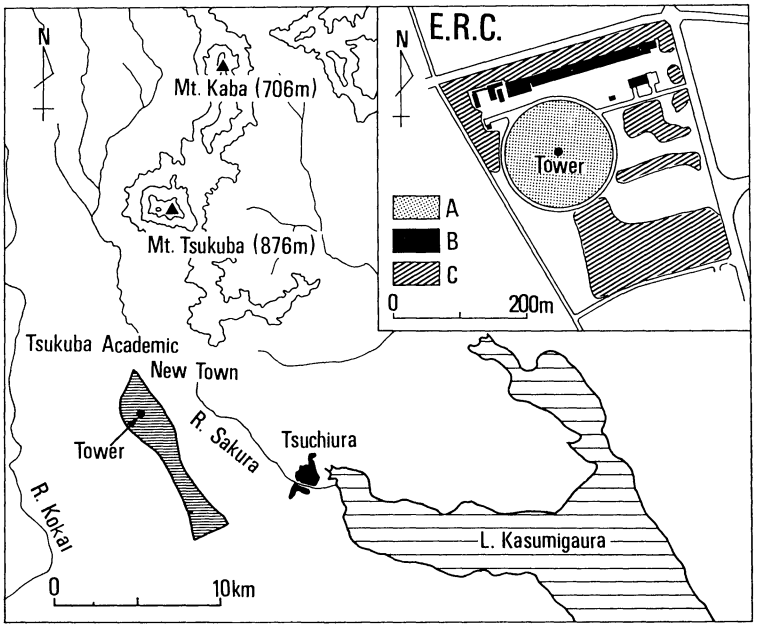

Fig. 2 Location of the experimental site. A=Grass field, B=Buildings, C=Coniferous wood.

havior of the turbulent energy budget under stable conditions as well as under unstable conditions.

2. Experimental methods

2.1 Experimental site and instrumentation

The site is the hydrometeorological observation field of the Environmental Research Center (ERC), the University of Tsukuba, at Sakuramura, Ibaraki-ken, Japan (36°06′N, 140°06′E; see Fig. 2). The field is circular in shape with a radius of 80 m and is covered by grass about 50 cm tall. The neighboring area is not completely homogeneous due to some buildings and forests, which are about 10 m in height. The 30 m tower was built at the center of the circular field. Fig. 3 shows a horizontal cross section of the 1 m square lattice-type tower with boom arrangements for the sonic anemometers and the resistance thermometers at the levels of 1.6, 4.3, 12.3 and 29.5 m above the ground. The booms for the four sonic anemometers extended 2.0 m to southeast. The desired wind direction for data collection was from southeast, to avoid distorting influences of the tower structure on the wind sensors. The booms for the resistance thermometers extended 2.0 m to northeast.

Fluctuating velocity components and temperature fluctuations were measured with three components sonic anemometer-thermometers (Kaijō Denki Model PAT 311). The sensing head of the anemometer has three 20 cm sound paths to measure the wind, one for the vertical component and two for the horizontal components. The frequency response of the sensors is about 20 Hz. The output signals from these sensors were transmitted through cables to a building outside the field and recorded on a computer-controlled data acquisition system (Kaijō Denki Model GP-1100). The signals were continuously monitored on chart recorders.

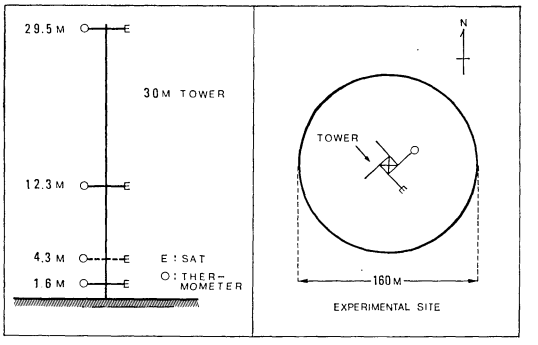

Fig. 3 30 m tower and the arrangement of sensors.

2.2 Data collection and reduction

The experimental runs are listed in Table 2.

Table 2 Selected runs for analysis.

Run No.	Date	Starting time (h·m)	$\bar{U}_{2.95m}$ (m/s)	WD	$\bar{T}_{1.6m}$ (°C)	Stability	Duration (min)
760	7/26/79	1100	3.5	E	28.1	Unstable	90
770	〃	1240	4.3	E	29.8	〃	〃
780	〃	1420	5.3	E	29.2	Neutral	〃
790	〃	2302	2.1	E	23.1	Stable	〃
830	7/29/79	2220	2.4	ESE	24.1	〃	〃
980	8/ 1/79	1400	5.0	SSW	31.2	Neutral	〃

Data collection was restricted to periods when the wind was mainly from southeast and constant in speed and direction. An experimental period was terminated when either wind speed or direction became unfavorable, to avoid the tower influence on wind speed measurements and the effect of nonstationarity.

A typical run length was 90 min, occasionally shortened to 10, 30 or 60 min during the actual experiment or during subsequent analyses. The basic averaged period used for the statistical analyses was 10 min. The mean and linear trend were removed from the turbulent velocity and temperature signals in order to reduce the effect of ultra-low-frequency fluctuations. Unless otherwise noted, the results to be presented will be based on the basic 30 min-averaged data which is the average of three consecutive 10 min-averaged groups of data.

Analog signals from the sonic anemometer-termometers were sampled 20 times a second, digitized and stored on magnetic tapes by means of the data acquisition system. The data were filtered with a band-pass digital filter with a frequency range from 0.0024 to 10 Hz in order to give good spectral resolution and to minimize the effect of aliasing.

Turbulence statistics, such as variances, covariances, triple moments and their gradients were computed directly from the simultaneously-sampled time series of u, v, w and θ, which represent the departures of the longitudinal, lateral and vertical velocity components and temperature from their respective means. The power spectra of the turbulent velocity and temperature were obtained using the Fast Fourier Transform (Hino, 1977). They were used to estimate the dissipation rate.

3. Theoretical relations and methods of analysis

3.1 Basic parameters

The Reynolds stress τ and the sensible heat flux H were determined by the eddy-correlation method, respectively:

$$\tau = -\rho\overline{uw} \tag{2}$$

$$H = \rho c_p \overline{w\theta} \tag{3}$$

The estimates of viscous dissipation ε were calculated from the spectra of the velocity components, by fitting the $-5/3$ power law, according to the Kolmogorov's theory for the inertial subrange,

$$\varepsilon = \left\{\frac{S_i(\kappa)\kappa^{5/3}}{A_i}\right\}^{3/2}, \quad \kappa = 2\pi n/\bar{U} \tag{4}$$

where κ is the wavenumber, n is the frequency and $S_i(\kappa)$ is the spectra of the velocity components ($i = u, v, w$).

The following velocity, temperature and length scales were used as the basic paramter,

$$u_* = \sqrt{(\tau/\rho)}$$

$$T_* = -H/(\rho c_p u_*) \tag{5}$$

$$z \text{ and } L = -\frac{u_*^3 \rho c_p \bar{T}}{kgH}$$

where u_* is the friction velocity, T_* is the friction temperature, L is the Monin-Obukhov length, k is the Kármán constant and c_p is the specific heat of air at constant pressure.

According to the Monin-Obukhov similarity theory, the results have been analyzed in dimensionless form, using the dimensionless quantities:

z/L

Monin-Obukhov stability parameter

$$\phi_\varepsilon(z/L) = \frac{kz}{u_*^3}\varepsilon$$

dimensionless viscous dissipation of turbulent energy

$$\phi_M(z/L) = \frac{kz}{u_*}\frac{\partial \bar{U}}{\partial z}$$

dimensionless term of mechanical production of turbulent energy

$$\phi_B(z/L) = \frac{kz}{u_*^3}\frac{g}{\bar{T}}\overline{w\theta}$$

dimensionless term of buoyant production of turbulent energy

$$\phi_T(z/L)=\frac{kz}{u_*^3}\frac{\partial}{\partial z}\frac{\overline{wq^2}}{2}$$

dimensionless term of turbulent transport of turbulent energy

$$\phi_I(z/L)=\frac{kz}{u_*^3}I$$

dimensionless term of the imbalance

3.2 *The equations for the turbulent energy budget*

The assumptions of horizontal homogeneity and stationarity are primarily responsible for the simplification of Eq. (1) In the present study the pressure transport term was not measured because of the difficulty in measuring the fluctuating pressure. Errors in neglecting the pressure transport term and in assuming homogeneity and stationarity are combined in an imbalance term IM.

Incorporating these assumptions, we take as our model of the turbulent energy budget

$$-\overline{uw}\frac{\partial\bar{U}}{\partial z}+\frac{g}{\bar{T}}\overline{w\theta}-\frac{\partial}{\partial z}\frac{\overline{wq^2}}{2}-\varepsilon+I=0 \quad (6)$$

$$(MP)\quad (BP)\quad (TT)\quad (VD)(IM)$$

In the surface boundary layer, Eq. (6) may be conveniently be expressed in dimensionless form, by multiplying through by kz/u_*^3,

$$\frac{kz}{u_*}\frac{\partial\bar{U}}{\partial z}+\frac{kz}{u_*^3}\frac{g}{\bar{T}}\overline{w\theta}-\frac{kz}{u_*^3}\frac{\partial}{\partial z}\frac{\overline{wq^2}}{2}-\frac{kz}{u_*^3}\varepsilon+\frac{kz}{u_*^3}I=0$$

or

$$\phi_M(z/L)-z/L-\phi_T(z/L)-\phi_\varepsilon(z/L)+\phi_I(z/L)=0 \quad (7)$$

The Monin-Obukhov similarity theory predicts that the terms in the turbulent energy budget should be universal function of z/L, which will be determined experimentally and tested in the following section.

4. Results and discussion

Turbulent statistics were measured at the four levels (1.6, 4.3, 12.3, 29.5 m) of the tower. Table 3 gives the resulting data with respect to the 90-min mean. Six runs were selected as representative of typical conditions during the experiment and were classified into three stability groups; Run 760 and 770, which represent unstable conditions, and Run 780 and 980, which represent almost neutral conditions, and Run 790 and 830, which represent stable conditions.

As evident from the site description in Section 2, the surface roughness up-wind of the tower was not completely homogeneous. This affected the measurements of wind profiles at the tower; the wind profiles showed the double-logarithmic structure. The air close to the ground was strongly influenced by this effect, so that the values at the lower level were omitted from the budget of turbulent energy. The values of each term in Eq. (7) were evaluated in the following two layers;

(1) a layer between the levels of 12.3 and 29.5 m
(2) a layer between the levels of 4.3 and 29.5 m

In all cases we refer to the terms on the left on Eq. (7), and if a term represent an energy gain, it is positive.

We now proceed to a discussion of the behavior of the terms in Eq. (7) at all stabilities. The results are summarized by the Monin-Obukhov similarity theory for comparison with previous studies.

4.1 *Viscous dissipation and spectra*

The spectra were computed using the Fast Fourier Transform. The resulting spectra were obtained by dividing each 90-min record into 9 consecutive 10-min blocks of data and constructing composite spectra by averaging the 9 separate spectra. The composite spectrum was then smoothed by averaging spectral estimates over frequency band.

The results of this experiment provide an opportunity to examine Kolmogorov's hypothesis for the behavior of the spectra in the inertial subrange. Fig. 4 shows the spectra for the longitudinal component u and for the vertical component w at the four levels of the tower, which are plotted in a log-log representation against frequency n (Hz) and divided into three groups according to the stability parameters z/L indicated in the figure. The broken line in the figure has a slope of $-5/3$ corresponding to Kolmogorov's hypothesis. The levels of the u- and w-spectra for near neutral conditions are higher than those for stable conditions. The spectra of u and w show a well-developed $-5/3$ slope of the inertial subrange on the high-frequency side. The u-spectra are found to obey the $-5/3$

Table 3 Turbulence statistics (with respect to the 90-min mean) at the four levels of the tower. Each run is classified into three stability groups according to z/L.

Run No.		Unstable			Neutral			Stable		
	z (m)	760	770	Mean	780	980	Mean	790	830	Mean
z/L	1.6	−0.12	−0.12	−0.12	−0.05	−0.04	−0.04	0.15	0.18	0.16
	4.3	−0.16	−0.22	−0.19	−0.05	−0.05	−0.05	0.17	0.34	0.26
	12.3	−0.18	−0.20	−0.19	−0.03	−0.08	−0.05	0.09	0.68	0.39
	29.5	−0.27	−0.25	−0.26	−0.07	−0.07	−0.07	1.03	3.21	2.12
$\bar{U}$ (m/s)	1.6	2.20	2.53	2.37	2.86	2.95	2.91	1.07	1.18	1.13
	4.3	2.49	2.90	2.70	3.32	3.49	3.41	1.14	1.29	1.22
	12.3	2.96	3.42	3.19	3.99	4.27	4.13	1.55	1.79	1.67
	29.5	3.51	4.37	3.94	5.30	5.04	5.17	2.13	2.42	2.28
$\bar{T}$ (°C)	1.6	28.1	29.8	29.0	29.1	31.2	30.2	23.1	24.1	23.6
u_* (m/s)	1.6	0.22	0.26	0.24	0.29	0.30	0.29	0.09	0.11	0.10
	4.3	0.28	0.32	0.30	0.38	0.42	0.40	0.12	0.14	0.13
	12.3	3.36	0.47	0.42	0.56	0.50	0.53	0.17	0.17	0.17
	29.5	0.32	0.40	0.36	0.41	0.56	0.49	0.15	0.14	0.15
$\overline{q^2}/2$ (m²/s²)	1.6	0.54	0.79	0.67	0.89	1.07	0.98	0.09	0.11	0.10
	4.3	0.62	0.92	0.77	1.05	1.24	1.15	0.11	0.14	0.13
	12.3	0.69	1.04	0.87	1.25	1.52	1.39	0.14	0.19	0.17
	29.5	0.70	0.99	0.84	1.07	1.49	1.28	0.14	0.19	0.16
σ_u (m/s)	1.6	0.63	0.76	0.69	0.84	1.01	0.93	0.29	0.31	0.39
	4.3	0.66	0.83	0.75	0.92	1.07	1.00	0.33	0.34	0.34
	12.3	0.72	0.89	0.81	1.00	1.18	1.09	0.34	0.41	0.38
	29.5	0.71	0.85	0.78	0.95	1.17	1.06	0.35	0.39	0.37
σ_v (m/s)	1.6	0.75	0.91	0.83	0.95	0.95	0.95	0.27	0.30	0.29
	4.3	0.76	0.92	0.84	0.95	0.96	0.96	0.27	0.33	0.30
	12.3	0.74	0.92	0.83	0.97	1.02	1.00	0.32	0.36	0.34
	29.5	0.74	0.91	0.83	0.90	0.96	0.93	0.31	0.37	0.34
σ_w (m/s)	1.6	0.32	0.39	0.35	0.41	0.44	0.43	0.15	0.17	0.16
	4.3	0.44	0.52	0.48	0.58	0.62	0.60	0.20	0.23	0.22
	12.3	0.53	0.65	0.59	0.73	0.76	0.75	0.25	0.27	0.26
	29.5	0.53	0.63	0.58	0.65	0.80	0.72	0.24	0.28	0.26
σ_T (°C)	1.6	0.55	0.66	0.60	0.49	0.45	0.47	0.22	0.24	0.23
	4.3	0.41	0.50	0.45	0.40	0.42	0.41	0.19	0.24	0.22
	12.3	0.34	0.42	0.38	0.38	0.42	0.40	0.21	0.26	0.24
	29.5	0.32	0.38	0.35	0.35	0.40	0.38	0.21	0.25	0.23

power law at much lower frequencies than the w-spectra. The position of the inertial subrange shifts to lower frequencies as increasing height. These results indicate that the horizontal scale of turbulence is larger than the vertical one and that the scale of turbulence increases with height.

Viscous dissipation is most important among the terms in the budget equation. As mentioned above, the estimates of viscous dissipation were obtained by assuming that Kolmogorov's hypothesis was valid. The $-5/3$ power law was fitted to u, v, w spectra and ε is evaluated for each with $A_u=0.50$ and $A_w=0.67$ (Haugen, 1973). Fig. 5 compares the estimate ε_u obtained from the u-spectrum with the estimate ε_w from the w spectrum. As can be seen in the figure, the agreement between ε_u and ε_w is good, so that ε_u is used as the estimate of ε.

Fig. 6 shows viscous dissipation as a function of mean wind speed at the four levels. From the figure, viscous disssipation increases with the third power of mean wind speed at a given height, but decreases with increasing height along the tower. The relation between ε and $\bar{U}$ at each level is expressed as follows:

$$\begin{aligned} \varepsilon &= 16.5\bar{U}^3 \quad \text{at} \quad 1.6\ \text{m} \\ \varepsilon &= 8.3\bar{U}^3 \quad \text{at} \quad 4.3\ \text{m} \\ \varepsilon &= 4.7\bar{U}^3 \quad \text{at} \quad 12.3\ \text{m} \\ \varepsilon &= 1.2\bar{U}^3 \quad \text{at} \quad 29.5\ \text{m} \end{aligned} \qquad (8)$$

Assuming the neutral case of Eq. (6), the following equation may be obtained:

$$\varepsilon=\frac{u_*^3}{kz}\phi_M(z/L) \qquad (9)$$

where ϕ_M is a function of stability z/L, and is unity when $z/L=0$. Eq. (9) leads the approximate result that for neutral conditions viscous dissipation equals mechanical production. Fig. 7 shows the relationship between ε and u_*^3/kz. It may be seen that there is some scatter in the figure because of the difference of stability, but one-to-one relationship exists between ε and u_*^3/kz for the cases of near neutral conditions. In near neutral conditions, mechanical production is a good measure of viscous dissipation.

In order to examine the scatter seen in Fig. 7, ε normalized by u_*^3/kz is plotted against stability z/L in Fig. 8. The solid curve is fitted to the data, and the dashed curve was obtained by Wyngaard and Coté (1971). The fitted through

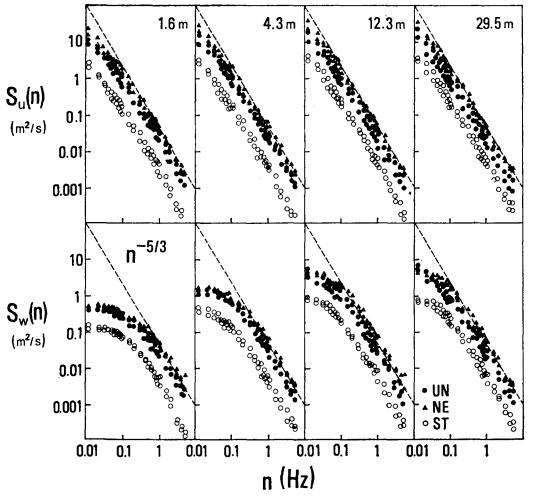

Fig. 4 Spectra of the velocity components, $S_i(n)$ $(i=u, w)$ at the four levels of the tower. Each run is classified into three stability groups according to the stability parameter z/L as follows: ●=unstable conditions, ▲=neutral conditions, ○=stable conditions. Each point represent a 90-min average.

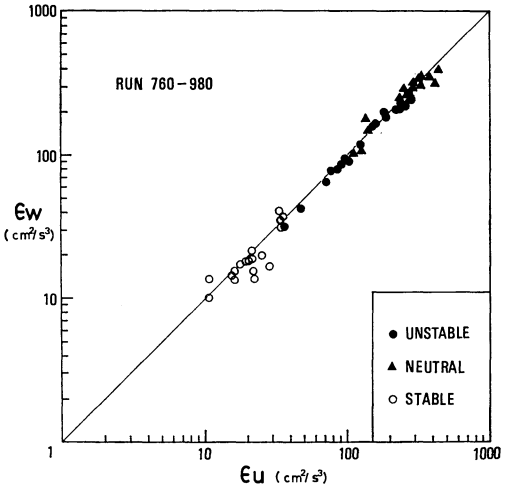

Fig. 5 Comparison of the estimate of viscous dissipation obtained by the u-spectrum in the inertial subrange with that obtained by the w-spectrum.

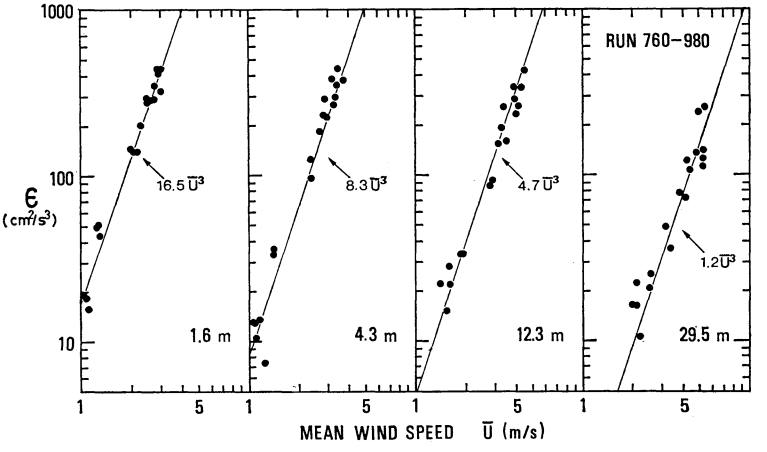

Fig. 6 Viscous dissipation as a function of mean wind speed at the four levels of the tower.

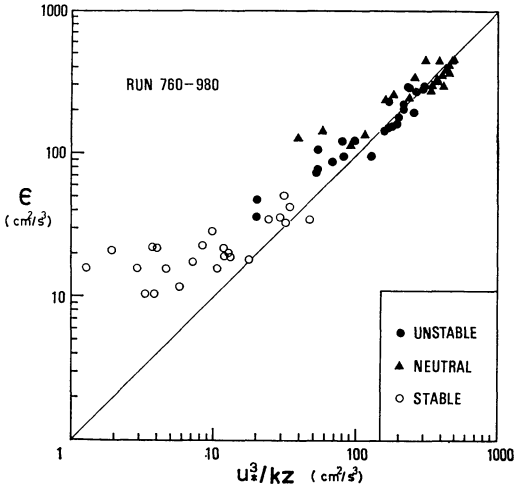

Fig. 7 Comparison of the measured viscous dissipation ϵ under various stabilities with the mechanical production of turbulent energy for neutral conditions, u_*^3/kz. Symbols are the same as those in Fig. 4.

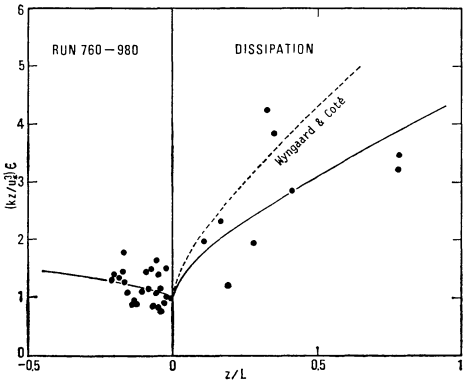

Fig. 8 Dimensionless viscous dissipation plotted against the stability parameter z/L.

the unstable data has the form

$$\phi_\epsilon(z/L)=(1+0.6|z/L|^{2/3})^{3/2} \quad (10)$$

The curve had been assumed to go through 1.0 at $z/L=0$. The curve fitted through the stable data has the form

$$\phi_\epsilon(z/L)=\{1-1.7(z/L)^{3/5}\}^{3/2} \quad (11)$$

The other investigators proposed the equations for viscous dissipation as follows:

Wyngaard and Coté (1971)

$$\phi_\epsilon(z/L)=(1+0.5|z/L|^{2/3})^{3/2} \quad (z/L<0)$$
$$=\{1+2.5(z/L)^{3/5}\}^{3/2} \quad (z/L>0) \quad (12)$$

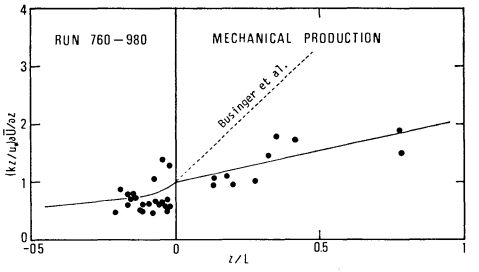

Fig. 9 Dimensionless rate of mechanical production of turbulent energy plotted against the stability parameter z/L.

Busch and Panofsky (1968)

$$\phi_\epsilon(z/L)=1+9z/L \quad (z/L>0) \quad (13)$$

Garratt (1972)

$$\phi_\epsilon(z/L)=(1-16z/L)^{-1/4}-z/L \quad (z/L<0)$$
$$=1+4z/L \quad (z/L>0) \quad (14)$$

Results for viscous dissipation are generally consistent with the previous results. The relation for unstable conditions is approximated by the formula as obtained by Wyngaard and Coté (1971) from the Kansas results. On the stable side, viscous dissipation is slightly small as compared with Wyngaard and Coté's results.

4.2 Mechanical production

Measurements of the dimensionless rate of mechanical production are shown in Fig. 9. The average properties of this curve should be those of the dimensionless wind shear $\phi_M(z/L)$, where

$$\phi_M(z/L)=\frac{kz}{u_*}\frac{\partial \bar{U}}{\partial z} \quad (15)$$

The curve fitted through the unstable data has the form

$$\phi_M(z/L)=(1-17z/L)^{-1/4} \quad (16)$$

Under stable conditions, the form of the curve is

$$\phi_M(z/L)=1+1.1z/L \quad (17)$$

These interpolation formulas are shown in Fig. 9 as well as those obtained by Businger et al. (1971).

It may be seen that the relation on the unstable side is approximated by the formula as obtained by Businger et al. (1971). But mechanical production on the stable side is systematically small by a factor of almost two. This difference may be explained by the fact that the

wind profiles at the tower are influenced by more or less inhomogeneous terrain.

4.3 Buoyant production

Buoyant production is simply normalized as

$$\phi_B(z/L) = -z/L \qquad (18)$$

and is a gain under unstable conditions and a loss under stable conditions.

4.4 The flux of turbulent energy and turbulent transport

In this section we examine the flux of turbulent energy and its divergence, or tubulent transport. Fig. 10 shows the relation between $\overline{wq^2}/2$ and u_* for the case of $\overline{wq^2}/2>0$. This shows that $\overline{wq^2}/2$ increases rapidly with the third power of u_*.

The dimensionless flux of turbulent energy $\overline{wq^2}/2u_*^3$ is plotted against the stability parameter z/L in Fig. 11. The results show a marked trend with z/L for unstable conditions, though there is no trend in stable conditions. The flux of turbulent energy is positive in most unstable cases. This feature implies upward energy transport, particularly in unstable conditions. In Fig. 11, the results are compared with the results from three other studies (Garratt, 1972; Wyngaard and Coté, 1971; Banke and Smith, 1973).

Turbulent transport were estimated by approximating the vertical derivative of $\overline{wq^2}/2$. The results show some evidence of obeying similarity on the unstable side, although the scatter is large (Fig. 12). The solid line in the figure is a fit to the data on the unstable side. For unstable conditions, turbulent transport behaves approximately as

$$\phi_T(z/L) = 3\frac{z}{L} \qquad (19)$$

Some of the scatter in the figure is probably due to the crude derivative approximation. Also, part of the scatter is probably caused by the inherently large uncertainty in the third moments.

Turbulent transport on the stable side of Fig. 12 does not show any clear trend. There is scatter around zero for small z/L. At large z/L, almost all the estimates are smaller in magnitude

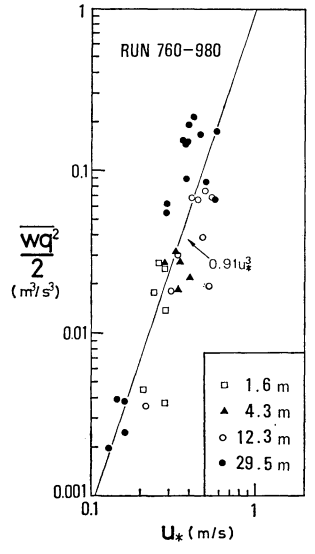

Fig. 10 Flux of turbulent energy plotted against the friction velocity. Symbols represent different heights as follows: □=1.6 m, ▲=4.3 m, ○=12.3 m, ●=29.5 m.

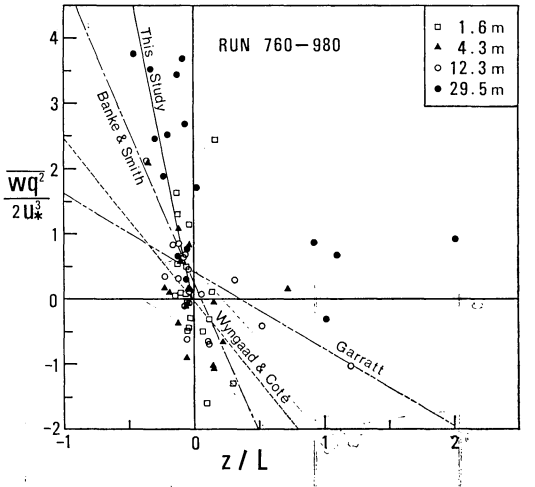

Fig. 11 Dimensionless flux of turbulent energy plotted against the stability parameter z/L. Symbols are the same as those in Fig. 10.

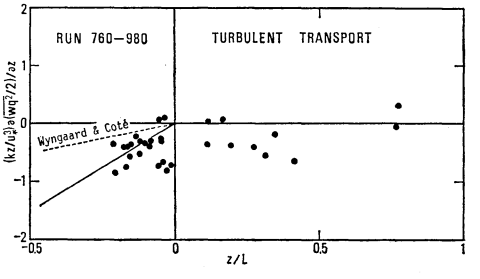

Fig. 12 Dimensionless rate of turbulent transport of turbulent energy plotted against the stability parameter z/L.

than z/L. It appears that turbulent transport is small compared to the dominant terms in the budget of turbulent energy.

4.5 The imbalance

The imbalance was calculated from the residual of the budget equation of turbulent energy. The dimensionless imbalance term is plotted against the stability parameter z/L in Fig. 13. Also plotted in the figure are the curves fitted to the data and the relation obtained by Wyngaard and Coté (1971). As can be seen from the figure, the imbalance is zero for near neutral conditions ($z/L \simeq 0$). As the magnitude of z/L increases, the imbalance becomes considerably larger.

As mentioned above, the assumptions on which the budget equation of turbulent energy (7) is based are not fully met by the ERC data. The imbalance shows the net contribution of the terms omitted from the equation. The accumulated errors of the measured terms, horizontal inhomogeneity, nonstationarity and pressure transport are involved in the imbalance. The result of the experiments indicates that the rate of change of turbulent energy is two order of magnitude too low, so that nonstationarity can be eliminated from consideration.

The large imbalance among the measured terms in the budget equation of turbulent energy under unstable conditions is discussed. The data show that with increasing instability there is an increase in the imbalance, and the imbalance is substantial. Wyngaard and Coté (1971) and Maitani (1977) had similar results. This implies that pressure transport is significant under very unstable conditions. The imbalance at $z/L = -0.5$ is about twice that of Wyngaard and Coté (1971). The horizontal inhomogeneity may account for this excess.

For very stable conditions, the imbalance is of the same order of magnitude as viscous dissipation, and larger than any of the other terms. As discussed above, mechanical production is underestimated because of horizontal inhomogeneity. This error could account for some of the imbalance under very stable conditions.

4.6 Vertical structure of the turbulent energy budget

Each term in Eq. (6) was computed for the data runs, and examples are shown in Fig. 14 for unstable conditions and Fig. 15 for stable conditions.

From Fig. 14, it is clear that for unstable conditions buoyant production and turbulent transport are approximately balanced, and also mechanical production decreases with increasing height and the absolute value of viscous dissipa-

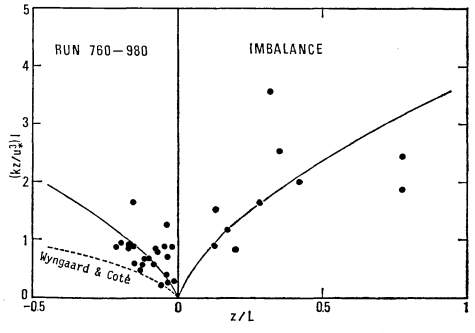

Fig. 13 Dimensionless imbalance of the turbulent energy budget plotted against the stability parameter z/L.

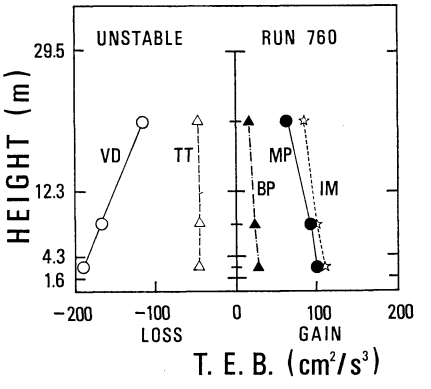

Fig. 14 Vertical structure of the turbulent energy budget in unstable conditions.

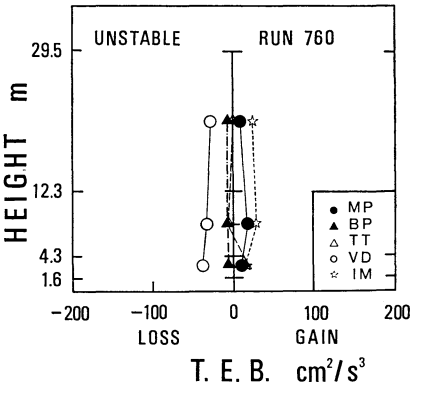

Fig. 15 As in Fig. 14 except for stable conditions.

tion decreases with height. Mechanical and buoyant productions are sources of turbulent energy. The former is much larger than the latter. Viscous dissipation and turbulent transport are energy sinks. The fact that turbulent transport is an energy sink means that near the surface, energy is exported upward by turbulence at double the rate it is produced by buoyancy. Viscous dissipation and mechanical production decrease markedly with height. This is caused by the effect of the surface boundary.

For stable conditions, each term of the turbulent energy budget is very small as compared with that for unstable conditions, and is almost constant with height (Fig. 15). Mechanical production and the imbalance are energy sources and the others sinks.

It can be concluded from Fig. 14 and Fig. 15 that mechanical production and viscous dissipation are a main energy source and sink, respectively. They decrease with height. Turbulent transport is an energy sink to approximately balance buoyant production which may be a source or sink depending on stability. Viscous dissipation exceeds the sum of mechanical and buoyant productions, and the imbalance is a gain and of the same order of magnitude as mechanical production. For stable conditions, the magnitude of each term is very small and almost constant with height.

4.7 Model

The model of the turbulent energy budget was deduced from the results. Fig. 16 shows the trend lines of all terms in the budget equation (7) against z/L. In neutral conditions, mechanical production and viscous dissipation are approximately in balance, while turbulent transport and buoyant production are not important. The imbalance is zero. In unstable conditions, each term in the budget equation is significant, and buoyant production is a gain. In this case the imbalance increases with the magnitude of absolute stability. Mechanical production becomes less important as instability increases, and buoyant production assumes a dominant role as the energy source. In addition, energy is exported upward by turbulence (turbulent transport) at triple the rate it is produced by buoyancy. In stable conditions, all terms except turbulent transport are significant, and buoyant production is a loss. For both stable and unstable conditions, the imbalance increases with the magnitude of absolute stability.

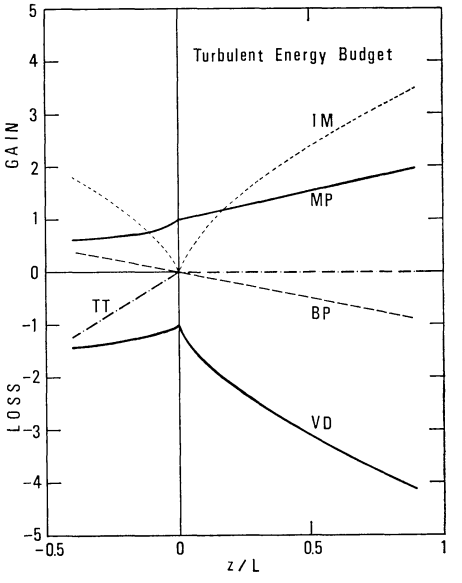

Fig. 16 A proposed model of the turbulent energy budget. Each term is dimensionless through multiplication by kz/u_*^3.

The general features of the model on the unstable side correspond approximately to those obtained by Wyngaard and Coté (1971). Some departures from them may be due to the surface roughness upwind of the tower.

Although the assumptions on which the budget equation of turbulent energy based are not fully met by the ERC data, the budget equation holds at the ERC tower under near neutral conditions, but fails during very stable and unstable conditions. The unmeasured term, which reflects possible horizontal inhomogeneity and pressure transport, may cause the large imbalance for very stable and unstable conditions. The investigation of this possibility must be the subject of further research.

5. Conclusions

Turbulence measurements of wind and temperature were made by sonic anemometer-thermometers in the first thirty meters of the atmosphere. This experiment has a detailed study of the turbulent energy budget in the surface boundary layer.

The behavior of each term in the budget equation of turbulent energy was examined in relation to stability and other parameters. The results are summarized as follows:

(1) Viscous dissipation increases with the third

power of mean wind speed, and decreases with height. For near neutral conditions, viscous dissipation is balanced with mechanical production.

(2) The flux of turbulent energy has a positive value, and increases with height. This trend is obvious for neutral and unstable conditions, but the flux is almost constant with height for stable conditions. The flux increases with the third power of friction velocity. The divergence of this flux, or turbulent transport shows some evidence of obeying similarity on the unstable side, although the scatter is large. Turbulent transport does not show any clear tendency on the stable side.

(3) The behavior of the imbalance can be expressed as a function of stability. The imbalance is zero for near neutral conditions. As the magnitude of stability increases, the imbalance becomes considerably large. The imbalance may be attributed to pressure transport (which was not measured) and/or to experimental difficulties such as horizontal inhomogeneity.

(4) The vertical structure of the turbulent energy budget was examined. For unstable conditions, mechanical production and viscous dissipation are a main energy source and sink, respectively. They decrease with height because of the surface boundary. Buoyant production is an energy source, and is smaller than mechanical production in the surface boundary layer. Turbulent transport is an energy sink. This means that near the surface, turbulent energy is exported upward by turbulence. For stable conditions, each term of the budget is very small as compared with that for unstable conditions, and is almost constant with height.

(5) A model of the turbulent energy budget was deduced from the results. A general specification of turbulent energy budget including the case of stable conditions has been achieved through the present model. Under near neutral conditions, mechanical production and viscous dissipation are dominant and essentially in balance, while turbulent transport and buoyant production are not important. In unstable conditions, each term in the budget is important, and buoyant production is a gain. In stable conditions, all terms except turbulent transport are significant, while buoyant production is a loss. Mechanical production and the imbalance are sources of turbulent energy and the others energy sinks. For both stable and unstable conditions the imbalance term increases with the magnitude of stability.

Acknowledgements

The author is grateful to Dr. M. M. Yoshino of the University of Tsukuba for many helpful suggestion and encouragements. The author is also grateful to Drs. T. Kawamura, T. Nishizawa and K. Kotoda of the University of Tsukuba for reviewing this paper. Frequent, stimulating and helpful discussion with Dr. T. Hanafusa of the Meteorological Research Institute are gratefully acknowledged. Thanks are due to Dr. M. Inokuchi, former Director of the Environmental Research Center, the University of Tsukuba for making available the experiment of which this paper is based. Thanks are also due to Dr. H. Tamiya of the Meteorological Research Institute and Mr. Y. Hayashi of the University of Tsukuba for many helpful suggestions, Mr. A. Yorisaki and Miss H. Takeuchi for their help in the preparation of the experiment and data reduction. The author is indebted to Mrs. P. Ogawa for a critical reading of the manuscript and my wife for typing the manuscript and drawing the figures. The computations in the present study were performed with use of the ACOS-800 computer at the Science Information Processing Center, the University of Tsukuba.

References

Banke, E. G. and S. D. Smith, 1973: Wind stress on arctic sea ice. *J. Geophys. Res.*, **78**, 7871-7883.

Busch, N. E. and H. A. Panofsky, 1968: Recent spectra of atmospheric turbulence. *Quart. J. Roy. Meteor. Soc.*, **94**, 132-148.

Businger, J. A., J. C. Wyngaard, Y. Izumi and E. F. Bradley, 1971: Flux-profile relationship in the atmospheric surface layer. *J. Atmos. Sci.*, **28**, 181-189.

Caughey, S. J. and J. C. Wyngaard, 1979: The turbulence kinetic energy budget in convective conditions. *Quart. J. Roy. Meteor. Soc.*, **105**, 231-239.

Champagne, F. H., C. A. Friehe and J. C. LaRue, 1977: Flux measurements, flux estimation techniques, and fine-scale turbulence measurements in the unstable surface layer over land. *J. Atmos. Sci.*, **34**, 515-530.

Elliott, J. A., 1972: Instrumentation for measuring static pressure fluctuations within the atmospheric boundary layer. *Boundary-Layer Meteor.*, **2**, 476-495.

Garratt, J. R., 1972: Studies of turbulence in the surface layer over water (Lough Neagh) Part

II. Production and dissipation of velocity and temperature fluctuations. *Quart. J. Roy. Meteor. Soc.*, **98**, 642-657.

Haugen, D. A. (ed.), 1973: Workshop on micrometeorology. American Meteor. Soc., 392 pp.

Hino, M., 1977: Spectral analysis (in Japanese). Asakura Shoten, 300 pp.

Kotoda, K., Y. Sakura, Y. Hayashi and K. Kai, 1978: On the observation and data acquisition system for the heat and water balance studies of ERC experimental field. Bull. Envir. Res. Center (Univ. of Tsukuba), **2**, 65-89.

Lenschow, D. H., 1970: Airplane measurements of planetary boundary layer structure. *J. Appl. Meteor.*, **9**, 874-884.

————, 1974: Model of the height variation of the turbulent kinetic energy budget in the unstable planetary boundary layer. *J. Atmos. Sci.*, **31**, 465-474.

Lumley, J. L. and H. A. Panofsky, 1964: The structure of atmospheric turbulence. John Wiley and Sons, Inc., 239 pp.

Maitani, T., 1977: Vertical transport of turbulent kinetic energy in the surface layer over a paddy field. *Boundary-Layer Meteor.*, **12**, 406-423.

McBean, G. A., R. W. Stewart and M. Miyake, 1971: The turbulent energy budget near the surface. *J. Geophys. Res.*, **76**, 6540-6549.

McBean, G. A. and J. A. Elliott, 1975: The vertical transports of energy by turbulence and pressure in the boundary layer. *J. Atmos. Sci.*, **32**, 753-766.

Monin, A. S. and A. M. Obukhov, 1954: Basic laws of turbulent mixing in the ground layer of the atmosphere. *Tr. Geofiz. Inst. Akad. Nauk SSSR*, **151**, 163-187.

Monji, N., 1973: Budgets of turbulent energy and temperature variance in the transition zone from forced to free convection. *J. Meteor. Soc. Japan*, **51**, 133-145.

Panofsky, H. A., 1962: The budget of turbulent energy in the lowest 100 meters. *J. Geophys. Res.*, **67**, 3161-3165.

Wyngaard, J. C. and O. R. Coté, 1971: The budgets of turbulent kinetic energy and temperature variance in the atmospheric surface layer. *J. Atmos. Sci.*, **28**, 190-201.

Yamamoto, S., O. Yokoyama and M. Gamo, 1979: Observational study on the turbulent structure of the atmospheric boundary layer under stable conditions. *J. Meteor. Soc. Japan*, **57**, 423-431.

接地層における乱流エネルギー収支

甲 斐 憲 次

筑波大学水理実験センター

筑波大学水理実験センターの気象観測塔の4高度（1.6, 4.3, 12.3, 29.5 m）に設置した超音波風速温度計による3次元の風速変動および温度変動の測定結果に基づき，乱流エネルギー収支式の各項を評価した。収支式は乱流の生成・消滅を原因別に分類したものであり，風速シアーによるエネルギーの生成項，浮力によるエネルギーの生成項，乱流輸送項，粘性消散項，残差項（圧力項を含む）よりなる。Monin-Obukhov の相似則を用いて収支式の各項と大気安定度との関数関係を実験的に求め，乱流エネルギー収支モデルを導いた。

乱流の統計的性質と乱流エネルギー収支を考察した結果，判明した事実は次の通りである。

1. 粘性消散項は平均風速の3乗に比例して増加し，高さと共に減少する。中立の場合，粘性消散項と風速シアー項は，ほぼバランスする。

2. 乱流エネルギー・フラックスは不安定の場合には正で高さと共に増加するが，安定の場合には高さと共にほぼ一定である。乱流輸送項は不安定の場合には浮力項の約2倍であるが，安定の場合にはほぼ零となる。

3. 測定できなかった圧力項のふるまいを示しているものと推察される残差項は，相似則に従い，大気安定度の関数として表わすことができる。中立の場合には残差項は零になるが，不安定および安定の場合には大気安定度の絶対値が増すにつれて残差項は増大する。

4. 乱流エネルギー収支の鉛直構造を調べた結果，大気安定度が不安定の場合には，風速シアー項と粘性消散項がそれぞれ主要な乱流エネルギーのソースとシンクである。両者は地表面の影響を受け，高さと共にその絶対値を減少する。浮力項もまたエネルギー・ソースであるが，その大きさは風速シアー項よりも小さい。乱流輸送項はエネルギー・シンクであるが，これは下層で生成された乱流エネルギーが上層に輸送されているものと考えられる。大気安定度が安定の場合には，収支式の各項は非常に小さくなり，高さと共にほぼ一定である。

5. 以上の結果より得られた乱流エネルギー収支モデルの概要は，次の通りである。大気安定度が中立の場合

には，乱流エネルギー収支は風速シアー項と粘性消散項のみで説明される。両者はほぼバランスし，他の収支項は零となる。安定領域では，浮力項は負に転じ，乱れを止めるように働く。エネルギー・ソースとしては，風速シアー項のみになる。安定度が増すと，乱流輸送項以外の収支項はその絶対値を増す。不安定領域では，不安定の度合が増すにつれて風速シアー項以外の収支項はその絶対値を増大し，浮力項がしだいにエネルギー・ソースとして重要になる。乱流輸送項はエネルギー・シンクとして重要になり，その大きさは浮力項の3倍程度である。